

Structural and Morphological Study of Silver Electrodeposits

Henrikas CESIULIS^{1*}, Oksana BERSIROVA², Aušra VALIŪNIENĖ¹,
Igoris PROSYČEVAS³, Gintaras BALTRŪNAS¹

¹Department of Physical Chemistry, Faculty of Chemistry, Vilnius University, Naugarduko 24, LT-2006, Vilnius, Lithuania

²V.I. Vernadski Institute of General & Inorganic Chemistry, Palladina 32-34, Kiev, 03-680, Ukraine

³Kaunas University of Technology, Institute of Physical Electronics, Savanoriu 271, Kaunas, Lithuania

Received 17 December 2003; accepted 03 June 2004

The structure and morphology of silver deposits obtained from 5 types of electroplating baths under predetermined optimal electrodeposition conditions have been studied. The deposits were formed from solutions: (a) 0.2 M $\text{KAg}(\text{CN})_2$ + 0.5 M KCN + 0.2 M KOH; (b) 0.2 M $\text{KAg}(\text{CN})_2$ + 2 M KCNS + 1 M K_2CO_3 ; (c) 0.13 M $\text{KAg}(\text{CN})_2$ + 0.82 M KH_2PO_4 + 0.41 M H_3BO_3 + 0.15 M K_2CO_3 + 0.69 M KOH; (d) 0.2 M AgNO_3 + 2.5 M NaCNS; (e) 0.3 M AgNO_3 + 2 M Na_2SO_3 . The obtained silver coatings as well as metallurgic silver were polycrystalline and nanocrystalline (the values of grain size were 36.9–56.5 nm). The peak broadening for electrodeposits is defined mainly by grain sizes whereas in metallurgic Ag one is governed by both grain sizes and microstrains. The deposits obtained from the baths in which thiocyanate or sulfite Ag(I) complexes were a source of silver contain all possible textures like in metallurgic silver, whereas deposits obtained from the baths in which $\text{Ag}(\text{CN})_2^-$ complexes were a source of Ag(I) does not contain texture (220) or corresponding peak is negligibly low. The values of lattice parameter and interplanar distance are provided. The roughness of electrodeposits was evaluated based on the STM examination and are in the range 34.3 nm to 80.8 nm.

Keywords: silver electroplating, electrodeposition, nanostructure, XRD, STM.

1. INTRODUCTION

The integrated circuits can be made smaller than 0.13 μm when using copper (Cu) as the interconnect material. Before, interconnects were made with other materials such as aluminum. In the sub 0.13 μm generation integrated circuits, copper will completely replace aluminum as the new interconnect material due to its favorable electrical conductivity (1.7 $\mu\Omega\text{ cm}$) and superior resistance to electromigration [1]. Note, the specific resistivity data corresponds to bulk material not for thin film layers. In the last case that data may vary from the bulk value dependently of their thickness [2]. Chips with more conductive Cu interconnect will operate consuming less power and at the significantly higher speeds due to decreased resistance-capacitance coupling delay. Silver is a very promising candidate for a new interconnects material because of its innate characteristics of having the lowest resistivity (1.6 $\mu\Omega\text{ cm}$) of all known common materials. Therefore, silver demonstrates attractive possibilities for application in microelectronics industry, e.g. for metals and alloys metallization [3–6] or for deposition on the barrier layers for ULSI applications [7–10], nanowires formation [11].

Structure and morphology govern a functionality of electrodeposits, and depend mainly on the kinetic parameters of the deposition process, and the deposition overpotential or current density, i.e. on the crystallization conditions. Obviously, the crystallization conditions might be different in various types of electroplating baths. The aim of present work is to examine morphology and structure of silver electrodeposits obtained from various

kinds of baths under predetermined optimal electroplating conditions.

2. EXPERIMENTAL

X-ray diffraction (XRD) analysis was performed for the characterization of electrodeposited coatings. Ni filtered $\text{Cu-K}\alpha_1$ radiation (30 kV and 30 mA, $\lambda = 1.54056 \text{ \AA}$) was used at a continuous scan speed of $0.02^\circ 2\theta \text{ s}^{-1}$. For most precise θ values for peaks and line broadenings determination the routines of the peak fitting using Gaussian- or Lorentzian- type functions were performed.

An STM instrument, NanoScope IIIa made by Digital Instruments, was used to examine a surface morphology and to estimate the roughness of the surfaces. The STM study was performed using the tunneling current up to 1 nA, the bias voltage – up to 300 mV, and the scanning rate of 0.9–2.0 Hz. The STM data obtained were further processed with computer software to produce 3-D images and to perform a roughness analysis.

Current density during experiments was controlled using a programmable galvanostat/potentiostat PI-50-1.1. Polished brass plates of working area 2 cm^2 were used as the substrates.

The silver electrodeposits were obtained from the following 5 different kinds of electroplating solutions based of $\text{KAg}(\text{CN})_2$ as a source of Ag(I) (baths 1–3), as well as pure non-cyanide solutions (baths 4–5) under following electrodeposition conditions:

1. **cyanide** [12]:

0.2 M $\text{KAg}(\text{CN})_2$ + 0.5 M KCN + 0.2 M KOH;
 $j = 5 \text{ mA cm}^{-2}$, $t = 20 \text{ }^\circ\text{C}$.

2. **dicyanoargentate-thiocyanate (DCAT)** [13–14]:

0.2 M $\text{KAg}(\text{CN})_2$ + 2 M KCNS + 1 M K_2CO_3 ;

*Corresponding author. Tel.: +370-5-2336419; fax.: +370-5-2330987.
E-mail address: henrikas.cesiulis@chf.vu.lt (H. Cesiulis)

$j = 5 \text{ mA cm}^{-2}$, $t = 20 \text{ }^\circ\text{C}$.

3. dicyanoargentate-borate-phosphate-carbonate (BPC) [3]:

0.13 M $\text{KAg}(\text{CN})_2$ + 0.82 M KH_2PO_4 + 0.41 M H_3BO_3 + 0.15 M K_2CO_3 + 0.69 M KOH ; $j = 5 \text{ mA cm}^{-2}$, $t = 55 \text{ }^\circ\text{C}$.

4. thiocyanate [6, 8 – 9]:

0.2 M AgNO_3 + 2.4 M NaCNS ;

$j = 5 \text{ mA cm}^{-2}$, $t = 20 \text{ }^\circ\text{C}$.

5. sulfite [15]:

0.3 M AgNO_3 + 2M Na_2SO_3 .

$j = 3 \text{ mA cm}^{-2}$, $t = 20 \text{ }^\circ\text{C}$.

3. RESULTS AND DISCUSSIONS

XRD study. Structural analysis of phases and other structural parameters of electroplated silver deposits and their comparisons with metallurgic silver were done using the XRD patterns that are shown in Fig. 1. The Miller indexes in the diffraction pattern were assigned to each peak based on the data presented in [16 – 17]. Evidently, the obtained silver coatings as well as metallurgic silver are polycrystalline. The ratios of intensities (I_{hkl}) of diffraction peaks are dependant on Ag-plating bath and are shown in Table 1. The deposits obtained from the baths in which thiocyanate or sulfite Ag(I) complexes are a source of silver contain all possible textures like in metallurgic silver, whereas deposits obtained from the baths in which $\text{Ag}(\text{CN})_2^-$ complexes are a source of silver (cyanide, DCAT and BPC) do not contain texture (220) (or corresponding peak is negligibly low (BPC bath)). Moreover, the textures (311) and (222) almost are absent in deposits, obtained from the BPC bath, and they consist mainly of phases (111) and (200). Metallurgic silver and electrodeposits obtained from the thiocyanate bath have preferential highest packing (111) orientation, whereas in other cases of electrodeposited silver two planes predominant, namely planes (111) and (200). Noticeable, that intensity of peak revealed to the plane (200) is highest for silver obtained from the sulfite bath, and it is almost equal to I_{111} for silver obtained from baths in which $\text{Ag}(\text{CN})_2^-$ is a source of silver (cyanide, DCAT and BPC baths).

As it is seen on Fig. 1, the corresponding values of $2\theta_{hkl}$ are different for metallurgic and electrodeposited silver. According to Bragg's law, the values of θ_{hkl} depend on the lattice parameter (a_0) and inter planar spacing (d_{hkl}) in a following way [18]:

$$\sin^2 \theta_{hkl} = \frac{\lambda^2}{4a_0^2} (h^2 + k^2 + l^2), \quad (1)$$

and for cubic crystals:

$$d_{hkl} = \frac{a_0}{\sqrt{h^2 + k^2 + l^2}}, \quad (2)$$

where λ is the X-ray wavelength (in Å); θ_{hkl} is a Bragg angle.

These parameters obtained for metallurgic silver and various electrodeposits are presented in Table 2. Based on these data, the average values of a_0 were determined for each kind of silver, and obtained data are shown in Fig. 2.

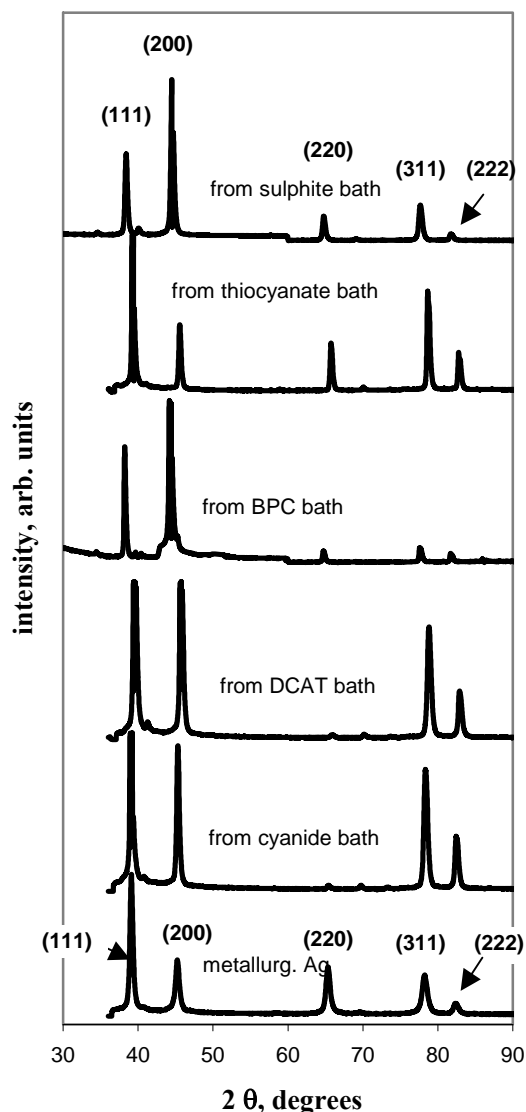


Fig. 1. The XRD patterns of metallurgic and electrodeposited silver. The types of electroplating baths are marked above spectra. Formulations and conditions of electrodeposition are presented in "Experimental"

Table 1. Diffraction peak intensities in the XRD patterns for metallurgic and electrodeposited silver

Ag obtaining method or bath	Intensities I_{hkl} of diffraction peaks (in arbitrary units)				
	I_{111}	I_{200}	I_{220}	I_{311}	I_{222}
Ag powder*	100	40	25	26	12
Metallurg.	100	40	33	26	7
From cyanide	100	94	~0	76	33
From DCAT	100	100	~0	70	33
From BPC	100	146	11	11	3
From thiocyanate	100	42	32	66	24
From sulfite	100	180	33	41	4

*According to data: Joint Committee on Powder Diffraction Standards (JCPDS).

Table 2. Lattice parameter (a_0) and interplanar spacing (d_{hkl}) for silver obtained by metallurgy and electroplated from various solutions

		Metallurg. Ag	From cyanide	From DCAT	From BPC	From thiocyanate	From sulfite
(111)	θ , deg	19.56	19.56	19.81	19.115	19.67	19.21
	d_{hkl} , Å	2.3008	2.3008	2.2729	2.3522	2.2884	2.3411
	a_0 , Å	3.9850	3.9850	3.9367	4.0742	3.9636	4.0548
(200)	θ , deg	22.63	22.66	22.90	22.17	22.79	22.29
	d_{hkl} , Å	2.0023	1.9994	1.9795	2.0413	1.9886	2.0313
	a_0 , Å	4.0046	3.9987	3.9590	4.0825	3.9771	4.0625
(220)	θ , deg	32.68	–	–	–	32.88	32.40
	d_{hkl} , Å	1.4266	–	–	–	1.4189	1.4376
	a_0 , Å	4.0350	–	–	–	4.0132	4.0660
(311)	θ , deg	39.12	39.18	39.41	38.80	39.33	38.85
	d_{hkl} , Å	1.2208	1.2193	1.2133	1.2293	1.2154	1.2280
	a_0 , Å	4.0490	4.0438	4.024	4.0771	4.0309	4.0727
(222)	θ , deg	41.16	41.27	41.45	–	41.45	40.91
	d_{hkl} , Å	1.1703	1.1678	1.1636	–	1.1636	1.1762
	a_0 , Å	4.0542	4.0453	4.0309	–	4.0309	4.0745

The silver deposits obtained from cyanide, DCAT and thiocyanate electroplating baths have a lattice parameter as 4.025 – 4.030 Å that is very close to metallurgic silver if standard deviation would be taken into account. In these cases the standard deviation did not exceed 0.035 Å. The electrodeposits obtained from the BPC and sulfite baths have a strained lattice with increased value of a_0 up to 4.078 Å (standard deviation 0.003 Å) regardless the predominating of high packing planes (111) and (200). Probably, this difference in a_0 values of thin films is caused by different orientation of nucleus at early growth stage dependently on the adsorption energy of ad-atoms to substrate and bonding energy between ad-atoms [17]. Probably, the differences in a_0 values define the different properties of deposits. For example, Ag obtained from the cyanide bath has similar to metallurgic Ag value of a_0 and posses similar to ones a corrosion behavior [19]. Whereas deposits obtained from BPC bath having deformed lattice posses lower corrosion resistance in comparison with metallurgic silver [4].

The calculation of grain size and dimensionless values of microstrain are performed by measuring the broadening of a particular peak in a diffraction pattern associated with a particular planar reflection from within the crystal unit cell. It is inversely related to the FWHM (full width at half maximum-broadening) of an individual peak- the more narrow the peak, the larger the crystallite size. For the grain size calculation the formula given originally by Scherrer:

$$\beta_{\tau} = \frac{K\lambda}{\tau \cos \theta_{hkl}} \quad (3)$$

where: β_{τ} is the peak broadening (in rad); K is the Scherrer factor and the digital constant as 0.94 is the best for cubic structure in the expression; τ is the grain size (in Å).

If this is the only reason for the broadening, then the value $\beta_{\tau} \cos \theta_{hkl}$ should be independent of the diffraction angle. However, the real situation is different, because of

the persistence of the additional stress-induced broadening β_{ε} which is given by the Wilson formula:

$$\beta_{\varepsilon} = 4\varepsilon \tan \theta_{hkl} \quad (4)$$

where ε is a dimensionless value („microstrain“).

The value of ε is usually assumed to be proportional to the square root of the density of dislocations. Note that “size” and “strain” broadening show different θ dependence. This provides a way to separate the two dependences. Assuming the shape of the line profiles to be of Gaussian form and both the grain size and microstrain contribute to the line broadening, the integral width, β , of the structurally broadened profile is given by [18]:

$$\beta^2 = \beta_{\tau}^2 + \beta_{\varepsilon}^2 = \left(\frac{K\lambda}{\tau \cos \theta} \right)^2 + (4\varepsilon \tan \theta)^2. \quad (5)$$

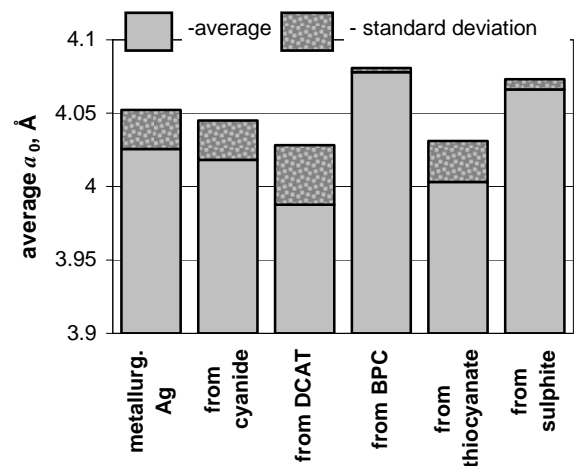


Fig. 2. Average values of lattice parameter (a_0) and evaluated standard deviation based on the data presented in Table 2

Plotting $\beta^2 \cos^2 \theta / (K\lambda)^2$ against $\sin^2 \theta / \lambda^2$ and extrapolating the line to $\sin^2 \theta / \lambda^2 = 0$ allows the estimation of K^2 / τ^2 and the slope of the line yields $16\varepsilon^2$, from which

the grain size τ and microstrain ε were calculated. The two characteristic sampling plots are presented in Fig. 3.

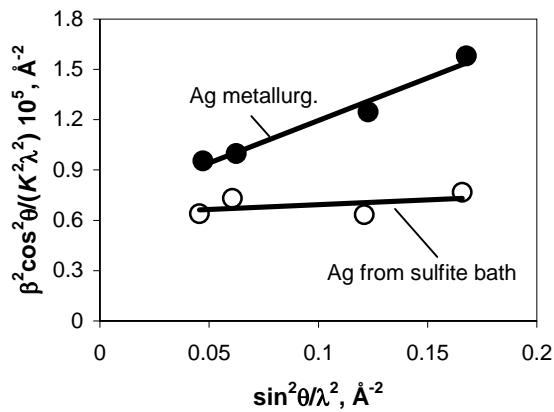


Fig. 3. Dependences for τ and ε evaluation (see text above)

As it is seen, for metallurgical silver the mentioned dependence is obtained in accordance with Eq. (5), i.e. linear growth ($\varepsilon=0.00177$) with argument increasing. In this case, the both two factors (grain size and microstrain) governed a XRD peak broadening. For silver obtained from sulfite baths as well as in other studied cases, the mentioned dependences are weaker and rather proof a scattered character of values. That could occur in one case, namely, if the XRD peaks broadening is governed just by grain size, whereas an effect of microstrain is negligible. The average values of grain size for metallurgical silver and electrodeposited from various kinds of baths are presented

in Table 3. As follows from the presented data, the obtained electrodeposits are nanocrystalline. The smallest grains are obtaining in metallurgical silver, but similar values were found also for silver electrodeposits obtained from DCAT, thiocyanate and sulfite solutions.

Table 3. The average grain sizes for silver obtained by metallurgy and electroplated from various solutions

Ag obtaining method or bath	Grain size, nm
Metallurgical Ag	35.9
From cyanide	44.1
From DCAT	36.9
From BPC	56.5
From thiocyanate	39.2
From sulfite	37.3

STM study. Morphology is probably the most important property of electrodeposited metals and it governs the applicability of each coating. The STM images of electrodeposits obtained from various baths are shown in Fig. 4. As it can be seen, excluding deposits obtained from the BPC baths, the surface of other deposits is less or more uniform and consists of homogeneously distributed grains. The surface of deposits obtained from BPC bath consists of coalesced grains with small fibers of 3 – 10 nm in length.

The roughness (R_a) was chosen as a quantitative parameter characterizing the morphology of surface, which is determined as arithmetic average of the absolute values of the surface height deviations measured from the mean plane.

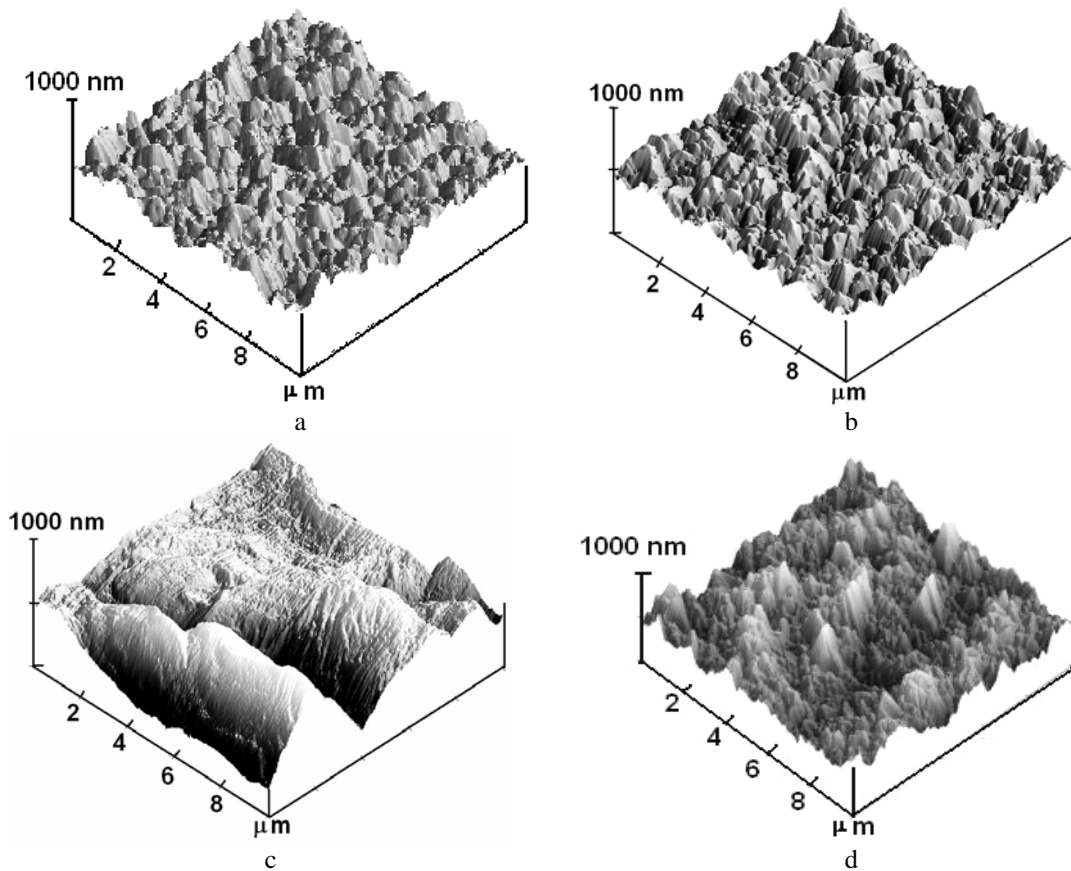


Fig. 4. Characteristic 3-D STM images of silver deposits obtained from various baths: a – from cyanide, b – from DCAT, c – from BPC, d – from sulfite. Formulations and conditions of electrodeposition are noted in “Experimental”

Table 4. The average roughness of substrate (polished brass) and silver deposits obtained by metallurgy and electroplated from various solutions (10 $\mu\text{m} \times 10 \mu\text{m}$ area scan)

Surface	Average roughness, nm
Substrate (polished brass)	4.5
From cyanide	39.5
From DCAT	34.3
From BPC	80.8
From thiocyanate	44.6
From sulfite	56.4

The values of average roughness obtained on the area scanned 10 $\mu\text{m} \times 10 \mu\text{m}$ for polished brass substrate and silver deposits are presented in Table 4. As it is seen, the minimal roughness is observed for the deposits obtained from cyanide and DCAT baths, and the highest was found for deposits obtained from BPC baths. It should be noted that the values of roughness well-correlate with lattice parameter of deposits: the less a_0 the less roughness.

4. CONCLUSIONS

1. Structural analysis of phases and other structural parameters of electroplated silver deposits were done based on the XRD patterns. The deposits obtained from the thiocyanate or sulfite baths contain all possible textures like of metallurgic silver, whereas deposits obtained from the cyanide, DCAT and BPC baths do not contain texture (220) or relevant peak is negligibly low. Moreover, the textures (311) and (222) almost are absent in deposits, obtained from the BPC bath.

2. The silver deposits obtained from cyanide, DCAT and thiocyanate electroplating baths have a lattice parameter and interplanar distance very close to metallurgic silver if standard deviation would be taken into account.

3. The obtained electrodeposits are nanocrystalline. The smallest grains are obtained in metallurgic silver, but similar values were found also for silver electrodeposits obtained from DCAT, thiocyanate and sulfite baths.

4. The minimal roughness (34 – 39 nm) is observed for the deposits obtained from cyanide and DCAT baths and highest as 81 nm was found for deposits obtained from BPC baths.

Acknowledgments

Authors acknowledge the Lithuanian Science and Study Foundation (grant C 03047) for partial financial support. O. Bersirova thanks to Ukrainian State Foundation for Fundamental Research under Ministry of Education and Science (grant No.03.07.117). Also, authors are grateful to Prof. Z. Stojek and Dr. M. Donten (University of Warsaw, Poland) for assistance performing STM examination.

REFERENCES

1. **Murarka, S. P., Verner, I. V., Gutmann, R. J.** Copper-Fundamental Mechanisms for Microelectronic Applications: Wiley Interscience, New York, 2000.
2. **Radoeva, M., Radoev, B.** Ohm Resistivity of Electroless Copper Layers as a Function of Their Thickness *J. Mat.Sci.* 30 (9) 1995: pp. 2215 – 2218.

3. **Bersirova, O., Kublanovsky, V., Emelianov, V., Anufriev, L.** Electrodeposition of Functional Silver Coatings from Borate-Phosphate-Carbonate Baths *Chemija* 1 2003: pp. 16 – 21.
4. **Bersirova, O., Królikowski, A., Kublanovsky, V.** Deposition Conditions and Corrosion Characteristics of Galvanic Silver Coatings for Microelectronics *J. Ochrona przed korozją* 11A 2002: pp. 149 – 152.
5. **Baltrunas, G., Cesiulis, H., Jankauskas, T., Survila, A.** Brilliance Maker for Silver and It's Alloys Electroplating. Pat. USSR N. 1419192.
6. **Cesiulis H., Jankauskas T.** Electrodeposition of Silver from Thiocyanate Solutions *Zashch. Pokrytiya Met.* 28 1994: pp. 26 – 29 (in Russian).
7. **Cheng, Ch., Arunagiri, T., Chyan, O.** Electrodeposition of Silver and Copper/Silver Multilayer on Ruthenium Substrate as a Potential New Metal Interconnect for Integrated Circuits *American J. Undergraduate Research* 2 (1) 2003: pp. 11 – 18.
8. **Cesiulis, H., Ziomek-Moroz, M.** Electrocrystallization and Electrodeposition of Silver on Titanium Nitride *J. Appl. Electrochem.* 30 (11) 2000: pp. 1261 – 1268.
9. **Cesiulis, H., Baltrunas, G.** Electrolytic and Contact Deposition of Silver onto Titanium Nitride *Materials Science (Medžiagotyra)* 7 (4) 2001: pp. 230 – 233.
10. **Cesiulis, H.** Modification of Titanium Nitride Surface by Silver *Theor. and Exper. Studies in Interfacial Phenom. and Technol. Applic. (Proceedings)* Lublin, Poland, 2003: pp. 31 – 33.
11. **Sauer, G., Brehm, G., Schneider, S.** Highly Ordered Monocrystalline Silver Nanowire Arrays *J. Appl. Physics* 91 (5) 2002: pp. 3243 – 3247.
12. **Baltrūnas, G., Pakalnie, E., Popkirov, G. S., Schindler, R.N.** The Surface Roughness of a Silver Electrode during Electrocrystallization in Cyanide Electroplating Bath *Z. Phys. Chem.* 216 2002: pp. 791 – 802.
13. **Baltrūnas, G., Jankauskas, T., Norkus, E.** Passivierung der Kathodenoberflächen während der Silberabscheidung aus cyanidischen Elektrolyten. Teil 1 *Galvanotechnik* 88 (10) 1997: pp. 3269 – 3278.
14. **Valkova, T., Krastev, I.** Electrodeposition of Silver from Thiocyanate-Cyanide Electrolytes Investigated by Cyclic Voltammetry *Trans.Inst.Met.Finish.* 80 (Part 1) 2002: pp. 13 – 15.
15. **Baltrunas, G., Valiuniene, A., Cesiulis, H.** Silver Electrodeposition from Sulfite Solutions *Materials Science (Medžiagotyra)* 7 (4) 2001: pp. 234 – 236.
16. **Jergel, M., Anopchenko, A., Majková, E., Spasova, M., Luby, Š., Holý, V., Brunel, M., Luches, A., Martino, M.** Excimer Laser Treated Ag/Co Multilayers Exhibiting Giant Magnetoresistance Effect *Superficies y Vacío* 9 1999: pp. 193 – 198.
17. **Yeon Sik Jung.** Study on Texture Evolution and Properties of Silver Thin Films Prepared by Sputtering Deposition *Appl. Surf. Sci.* 2003 (in press).
18. **Klug, H. P., Alexander, L. E.** X-Ray Diffraction Procedures for Polycrystalline and Amorphous Materials: Wiley Interscience, New York, 1974.
19. **Cesiulis, H., Ziomek-Moroz, M., Turcio-Ortega, D.** Corrosion Resistance of Silver and Silver Thin Films on TiN Substrate. – *51st Annual ISE Meeting*, 3 – 8 September, 2000, Warsaw, Poland, 534 p.
20. **Rosenberg, Yu., Machavariani, V. Sh, Voronel, A, Garber, S., Rubshtein, A., Frenkel, A. I., Stern, E. A.** Strain Energy Density in the X-ray Powder Diffraction from Mixed Crystals and Alloys *J. Phys.: Condens. Matter* 12 2000: pp. 8081 – 8088.